Characterization of Vertical Velocity and Drop Size Distribution Parameters in Widespread Precipitation at ARM Facilities

SCOTT E. GIANGRANDE AND EDWARD P. LUKE

Atmospheric Sciences Division, Brookhaven National Laboratory, Upton, New York

PAVLOS KOLLIAS

Department of Atmospheric and Oceanic Sciences, McGill University, Montreal, Quebec, Canada

(Manuscript received 26 October 2010, in final form 26 July 2011)

ABSTRACT

Extended, high-resolution measurements of vertical air motion and median volume drop diameter D0 in widespread precipitation from three diverse Atmospheric Radiation Measurement Program (ARM) locations [Lamont, Oklahoma, Southern Great Plains site (SGP); Niamey, Niger; and Black Forest, Germany] are presented. The analysis indicates a weak (0–10 cm^{-1}) downward air motion beneath the melting layer for all three regions, a magnitude that is to within the typical uncertainty of the retrieval methods. On average, the hourly estimated standard deviation of the vertical air motion is 0.25 m s^{-1} with no pronounced vertical structure. Profiles of D0 vary according to region and rainfall rate. The standard deviation of 1-min-averaged D0 profiles for isolated rainfall rate intervals is 0.3–0.4 mm. Additional insights into the form of the raindrop size distribution are provided using available dual-frequency Doppler velocity observations at SGP. The analysis suggests that gamma functions better explain paired velocity observations and radar retrievals for the Oklahoma dataset. This study will be useful in assessing uncertainties introduced in the measurement of precipitation parameters from ground-based and spaceborne remote sensors that are due to small-scale variability.

1. Introduction

Widespread large-scale precipitation, as viewed by operational weather radar systems, is commonly associated with prominent radar melting-layer signatures (e.g., bright band) and weak horizontal radar reflectivity gradients. These radar characteristics of widespread precipitation are often linked with slowly evolving drop size distributions (DSDs) and weak vertical air motions (e.g., Steiner et al. 1995; Houze 1997). Despite this slowly varying radar view, it is natural to expect some degree of physical process variability in space and time. Notably, variability within profiles of the DSD in light precipitation is considered a main source of uncertainty for several ''instantaneous'' (herein, referring to minute or shorter-term platform integration) radar-based remote retrievals of precipitation parameters. This includes those from the operational weather radar networks and spaceborne radar platforms such as the National Aeronautics and Space Administration (NASA) Tropical Rainfall Measuring Mission (TRMM), *CloudSat*, and the upcoming Global Precipitation Measurement program (GPM) and the European Space Agency's Earth Cloud Aerosols Radiation Explorer (EarthCARE) (e.g., Kummerow et al. 2000; L'Ecuyer and Stephens, 2002; Masunaga and Kummerow 2005). The majority of these existing and planned spaceborne radars operate at centimeter- and millimeter-wavelength frequencies wherein the radar view of precipitation provided is challenging because of non-Rayleigh and attenuation effects in rain (e.g., Kollias et al. 2007b).

Considerable advancement in characterizing DSD variability in rain has been gained through extensive work with surface disdrometer records (e.g., Joss and Waldvogel 1967). Recent studies reinforce that significant physical variability in rainfall rate and DSD parameters is present within typical scanning radar footprints [~1 km^3; e.g., Tokay and Short (1996), Miriovsky et al. (2004), Lee and Zawadzki (2005), and Tokay and Bashor (2010)]. However, disdrometers offer measurements at the surface

Corresponding author address: Scott Giangrande, Atmospheric Sciences Division, Brookhaven National Laboratory, Bldg. 490D, Bell Ave., Upton, NY 11973.
E-mail: scott.giangrande@bnl.gov

DOI: 10.1175/JAMC-D-10-05000.1

only (e.g., no profiling capabilities) and are prone to system and observational noise, in part because of their limited sampling (or catchment) volumes in space–time (e.g., Lee and Zawadzki 2005).

Radars and radar–wind profilers have extended sampling volumes for DSD observations (e.g., Campos and Zawadzki 2000; Cifelli et al. 2000; Bringi et al. 2009) and provide multidimensional storm insight (e.g., Yuter and Houze 1995; Williams et al. 2000). Akin to scanning weather radars benefiting from polarimetric moments for additional DSD bulk shape and media classification insight, profiling radars operating at 95 GHz may capitalize on non-Rayleigh backscattering signatures on radar Doppler spectra (Lhermitte 1987) and thus retrieve vertical air motion and DSD insight with height. Recently, such retrievals were automated for the 95-GHz radar systems of the Department of Energy's Atmospheric Radiation Measurement (ARM) Program (Giangrande et al. 2010). ARM cloud radar deployments in stratiform regimes include fixed-site operations at the Southern Great Plains (SGP) central facility in Lamont, Oklahoma, as well as campaign-style ARM Mobile Facility (AMF) deployments in the regions of Niamey, Niger (NIM), and Germany's Black Forest (FKB). A collocated 35-GHz (Ka band) radar at SGP allows cross comparisons for the performance of dual-frequency Doppler velocity-based DSD retrievals.

This paper explores the characteristics of high-resolution measurements of vertical air motion and median volume drop diameter (D0) retrieved using 95-GHz radar methods in widespread precipitation from three diverse ARM locations (SGP, NIM, and FKB). One goal is to gain insight into mean volume diameter profile variability in stratiform precipitation within spaceborne radar footprints. The paper is organized as follows. In section 2, we provide a brief description of the multisite deployment dataset and the ARM cloud radar systems. Additional details on the retrieval methods are also provided in section 2. Results for the three ARM locations are offered in section 3, with discussion and concluding remarks in section 4.

2. Dataset and methodology

a. ARM cloud radar datasets and Doppler spectra interpretation

1) ARM W-BAND 95-GHZ AND KA-BAND 35-GHZ CLOUD RADARS

The W-band ARM Cloud Radar (WACR) is a 95-GHz vertically pointing single-antenna Doppler radar that features a very short wavelength ($\lambda \approx 3.2$ mm) and is sensitive to small liquid droplets and ice crystals. For rainfall studies, the 1.2-m antenna provides a narrow beamwidth (0.19°) and the short temporal (4 s, with 2.14-s data integration) and spatial (42 m) resolutions make the radar suitable for the sampling of small atmospheric volumes at close distances. Added insight is obtained through a collocated 35-GHz (Ka band) vertically pointing Millimeter Cloud Radar (MMCR) at the SGP central facility (Kollias et al. 2007a). The MMCR 0.19° antenna beamwidth and spatial (45 m) and temporal (4 s) resolutions offer a solid match for dual-frequency work with the WACR. Although the WACR non-Rayleigh methods in this study are applicable under most rainfall rate conditions, we restrict our efforts to using ARM collocated rain gauge rainfall rates between 1 and 10 mm h^{-1} to highlight stratiform rain conditions (e.g., Nzeukou et al. 2004) and environments wherein full WACR retrieval coverage is typically observed to the base of the melting layer (stratiform rain criteria).

2) ARM SGP OKLAHOMA AND AMF NIAMEY/GERMANY

The Lamont SGP dataset for this study is a subset of a multiyear, continuous fixed-site ARM SGP WACR Doppler spectra record. This dataset includes dates between 1 May 2007 and 2 June 2007, having 85 h matching the stratiform rain criteria. This SGP dataset was previously highlighted for the testing of automatic retrievals as in Giangrande et al. (2010). It was observed that our stratiform rain criteria were often met within regions trailing deep convective storms (Houze 1997).

New datasets have been incorporated following 2006 and 2007 ARM AMF deployments. The tropical NIM 2006 AMF deployment covers the active West African wet monsoon months from 1 April through 30 September 2006 (175 h of observations). The FKB deployment was in conjunction with the Convective and Orographically Induced Precipitation Study (COPS; Wulfmeyer et al. 2008). The FKB record covered from 1 April through 30 September 2007 and favors long-duration precipitation regimes with typical melting-layer bottom heights below 2.5 km (156 h of observations).

The top panels in Figs. 1 and 2 show examples of reflectivity factor Z for characteristic events from the Niamey and Black Forest deployments, respectively. [For examples at SGP, including a cross comparison with Ka- and S-band systems, consult Giangrande et al. (2010).] Reflectivity fields indicate the prominent role of attenuation in rain at the W-band wavelength within deep convective cores and to above 1–2 km (e.g., complete extinction, as at NIM; Fig. 1). The radar coverage to altitude improves in widespread lighter precipitation regimes (rain rate < 5 mm h^{-1}).

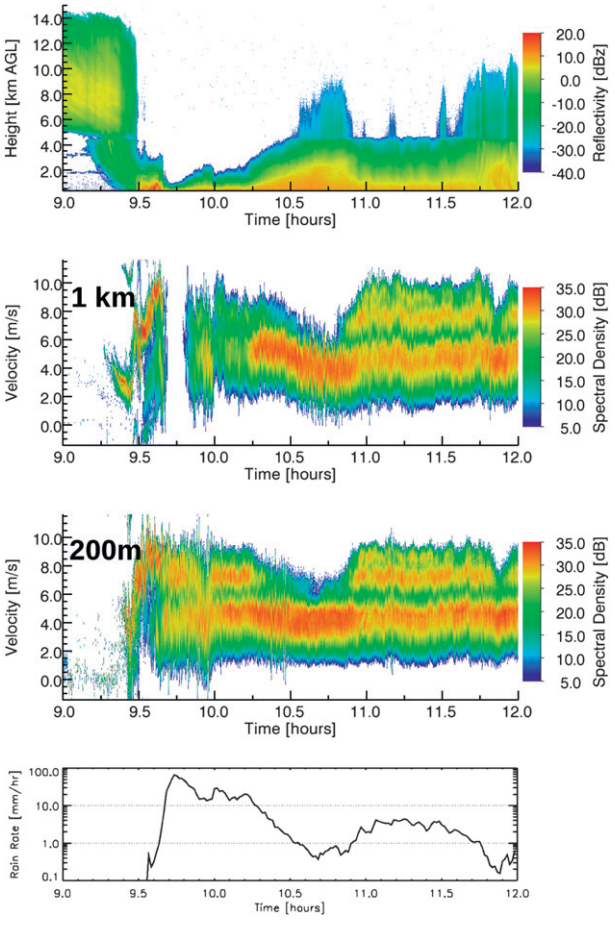

FIG. 1. (top) WACR reflectivity factor time–height plot for the 22 Jul 2006 deep convective storm at NIM. (middle two panels) Spectrograms (velocity along ordinate; spectral density in color) of WACR Doppler spectra at constant altitudes of 1 km and 200 m, respectively. (bottom) Rainfall rate from the collocated surface rain gauge (log$_y$ scale).

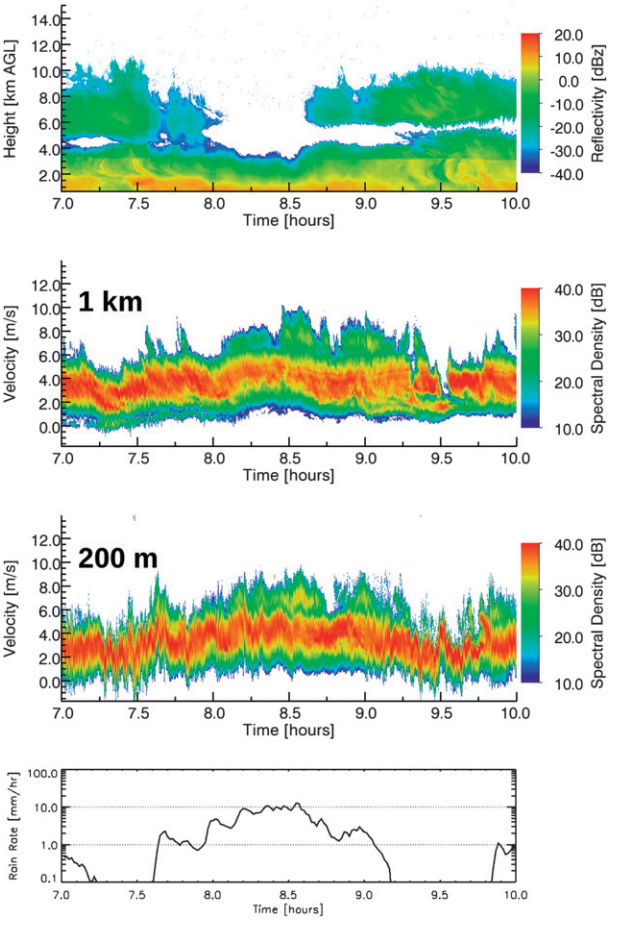

FIG. 2. As in Fig. 1, but for the event on 8 Aug 2007 at FKB.

3) INTERPRETATION OF WACR DOPPLER SPECTRA

In addition to standard radar moments including the reflectivity factor Z, the ARM archives Doppler spectra for all WACR campaigns including AMF deployments. For a vertically pointing radar system, the spectral density $S_d(v)$ of a given velocity bin for a Doppler spectrum is described as

$$S_d(v) = \sigma_b(D)N(D)\,dD/dv, \qquad (1)$$

where $N(D)$ is the number concentration and $\sigma_b(D)$ is the backscattering cross section of a raindrop with diameter D and a terminal fall velocity v. Doppler spectra as in (1) are widely treated for weather-type media as Gaussian-like features, although this behavior is not a necessity (e.g., Zrnić 1975). As highlighted by Lhermitte (1987), Doppler spectra at W band reflect unique insights into precipitation processes as a consequence of drop non-Rayleigh resonance effects on the backscatter cross section, as in (1). Under typical $N(D)$ behavior, these patterns are manifested as non-Gaussian, multimodal spectral features (as in time sequences; Figs. 3 and 4). Non-Rayleigh spectral characteristics are of particular interest within the context of precipitation studies since their appearance on the W-band Doppler spectra is largely unaffected by partial attenuation in rain.

A short introduction to the W-band rain Doppler spectrum and its potential use for velocity and DSD retrievals is provided below to facilitate data interpretation. From vertically pointing radar spectral measurements, it follows that faster Doppler fall velocities map monotonically to increasingly larger drop sizes (with ambient air motions and turbulence shifting and broadening the range of spectral velocities). In Figs. 1 and 2, panels beneath the Z time–height sequences illustrate WACR Doppler spectra and corresponding ground gauge rainfall

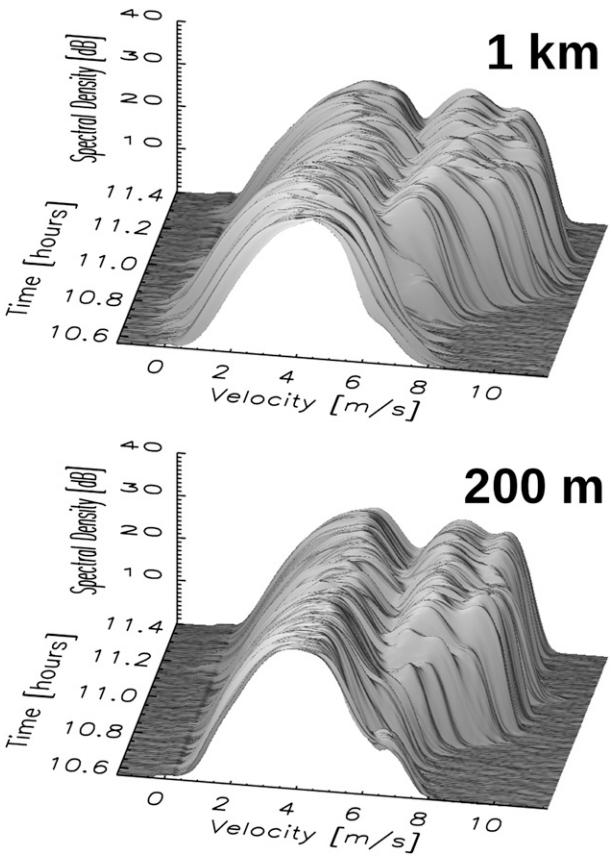

FIG. 3. Examples of the WACR Doppler spectra from the 22 Jul 2006 event at NIM for an hour-long sequence at two lower altitudes [(top) 1 km and (bottom) 200 m] through light–moderate precipitation ($R < 10$ mm h^{-1}).

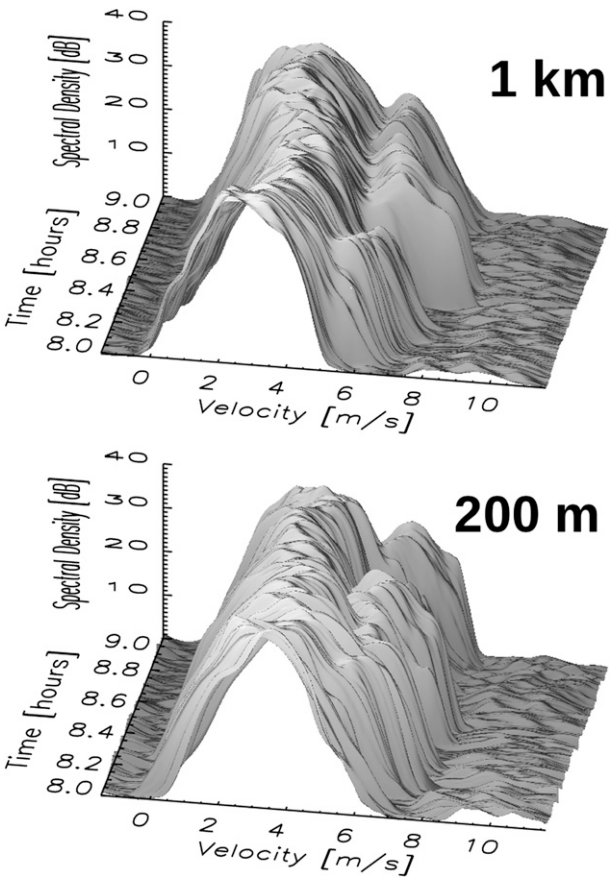

FIG. 4. As in Fig. 3, but for the 8 Aug 2007 event at FKB.

rate observations in time. The middle panels in Figs. 1 and 2 illustrate the Doppler spectra at two heights above ground level (1 km and 200 m). In these panels, spectral density has been mapped to a color scale (in arbitrary decibel magnitude above noise floor), with time placed on the abscissa and Doppler (fall) velocity represented by the ordinate. In Figs. 3 and 4, an hourly block of Doppler spectra associated with the events and altitudes from Figs. 1 and 2 have been plotted in the more traditional spectral fashion (velocity along the abscissa and spectral density for the ordinate). One should note the slight broadening of these Doppler spectra as a consequence of changes in air density with altitude.

As an example, Figs. 1 and 3 show the 22 July 2006 thunderstorm event at NIM. Visually, the frequently non-Gaussian (bi- or trimodal) spectra shape during most light–moderate precipitation is apparent. This multimodal behavior has known links to drop sizes associated with the maxima and minima in the radar backscatter cross section. As in Giangrande et al. (2010) automatic methods, this first minimum location is associated with the drop size $D \sim 1.65$ mm and is therefore useful as a "blueprint" for retrieving the mean air motion. The relative spectral location of this minimum fluctuates most during convective regions of the 22 July 2006 event wherein updrafts–downdrafts and turbulence are most pronounced.

Before considering more detailed DSD retrieval efforts using WACR spectra, it should be highlighted that the presence–absence and relative prominence of key spectral features qualitatively conveys information on the availability of certain bulk drop sizes in the illuminated radar volume. As in the NIM example from Figs. 1 and 3, the strong bimodality is not always present in the Doppler spectra with time. Prior to onset of the heaviest surface rainfall just after 0930 UTC on July 22, it is likely that drop sorting (preferential fall speed separation of drop sizes) is responsible for the very intense, narrow single spectral peak signatures that evolve into the classical bimodal characteristics. Following in time from left (deep convective core) to right (trailing stratiform) in Fig. 1, one may note the following. 1) The convective core is often bimodal (slightly larger second than first peak magnitudes), which indicates that small to medium

sizes under 2.5 mm dominate. One notes a total loss of Doppler spectral signatures at 1 km under the heaviest precipitation (just after 0930 UTC under $R > 60$ mm h^{-1} conditions) as a consequence of attenuation in rain. 2) A "transition zone" around 1030 UTC is present that exhibits a single, intense spectral peak (centered on drops approximately 1.1 mm in size), arguing for a lessened contribution from drops larger than 1.65 mm (e.g., no pronounced non-Rayleigh minimum). 3) A progression is evident toward trailing stratiform rain regimes with aggregation processes dominant. For times associated with the third effect, three spectral peaks are visible in Figs. 1 and 3 at mature widespread precipitation stages, which argues for the greater relative contribution from drop sizes larger than 2.5 mm in diameter based on physical drop backscatter cross-section arguments. The third peak is typically faint and narrow as compared with the first and second peaks.

b. Automatic DSD parameter retrieval methodology

1) DSD PARAMETER RETRIEVALS AT ARM/AMF FACILITIES

Retrievals of vertical air motion and DSD shape are performed using non-Rayleigh Doppler spectra inversion techniques for ARM WACR systems described in detail by Giangrande et al. (2010). Velocity retrieval methods are unchanged from previous non-Rayleigh descriptions in that manuscript. The primary requirement is an assumption for the terminal fall speed of that particular $D \sim 1.65$ mm drop size associated with the first non-Rayleigh Doppler spectra minima. Near surface conditions, these retrievals are expected to be accurate to within a few centimeters per second, limited primarily by the accuracy of the existing fits to Gunn and Kinzer's (1949) observations and radar spectral resolution. Aloft, an altitude correction to adjust for changes in the air density is necessary (e.g., Foote and du Toit 1969; Beard 1985). As in Giangrande et al. (2010), velocity correction assumes a behavior representative for this specific drop size and air density changes at altitude:

$$V = V_0\left(\frac{\rho_0}{\rho}\right)^n, \tag{2}$$

where ρ is the air density and the subscript reflects sea level conditions at which the Gunn and Kinzer (1949) observations are valid. The Giangrande et al. (2010) retrieval assigns an n coefficient of $n = 0.5$. The decision follows discussions from Lhermitte (2002, chapter 3.3.6) for better matching the behavior at altitude of smaller drop sizes. Coefficients for radar-based analysis in light–moderate rain [e.g., Beard (1985) relations, $n \sim 0.41$–0.45] and the standard Foote and du Toit (1969) value of $n = 0.4$ are slightly lower and at altitude imply a gradual offset on the order of 10 cm^{-1} (near melting-layer base). Here, the change weakens apparent downward motions at altitude as compared with applying standard coefficients.

Because the Giangrande et al. (2010) effort only considered a particular exponential form DSD parameter retrieval, a brief description toward a gamma model method of moments (M) DSD parameter estimate is also provided. Using standard assumptions for drop terminal fall speed and the backscatter cross section as discussed in Giangrande et al. (2010), (1) is solved for number concentration $N(D)$. Since the WACR spectral density is attenuated in rain, $N(D)$ is viable only as a relative measure of the number concentration. This relative $N(D)$ is sufficient to calculate DSD slope and shape.

Expressions for the moments for the $N(D)$ and gamma DSD solutions are as in Vivekanandan et al. (2004) and as generalized more recently by Cao and Zhang (2009, their appendix A). Any DSD model moment-based estimators, especially at the smaller drop size ends of the DSD, are subject to several known deficiencies (e.g., Cao and Zhang 2009). One should be selective when considering models that may offer sensitivity to specific small and large drop processes (e.g., gamma over exponential), noting that these models may be prone to additional errors in parameter estimates. For this study, complementary disdrometer observations were unavailable from AMF WACR deployments at NIM and FKB. Impact disdrometer observations were available at SGP, as documented in Giangrande et al. (2010). However, lack of a higher-quality video disdrometer record limits our ability to favor the error characteristics of a particular middle-moment exponential or gamma estimator (e.g., M234, M246, and M345) best matched to a WACR–disdrometer intercomparison. We adopt a standard truncated (incomplete) gamma model M246 retrieval following the Cao and Zhang (2009) recommendation, given its solid theoretical performance and previous track record as a robust technique for video disdrometers. A simplification is also performed following M246 retrievals wherein DSD shape μ and slope Λ retrievals are concatenated to terms of a bulk median volume drop diameter:

$$\mathrm{D0} = (\mu + 3.67)/\Lambda. \tag{3}$$

Since gamma retrievals may incorporate additional insight on smaller and larger drop size availabilities, there is potential benefit for these methods over previous M36 methods [where μ is assumed to be 0, as in Giangrande et al. (2010)]. Median drop sizes computed using M36 behave similarly to M246 retrievals with values biased low by 0.1–0.2 mm (not shown). Since the SGP impact

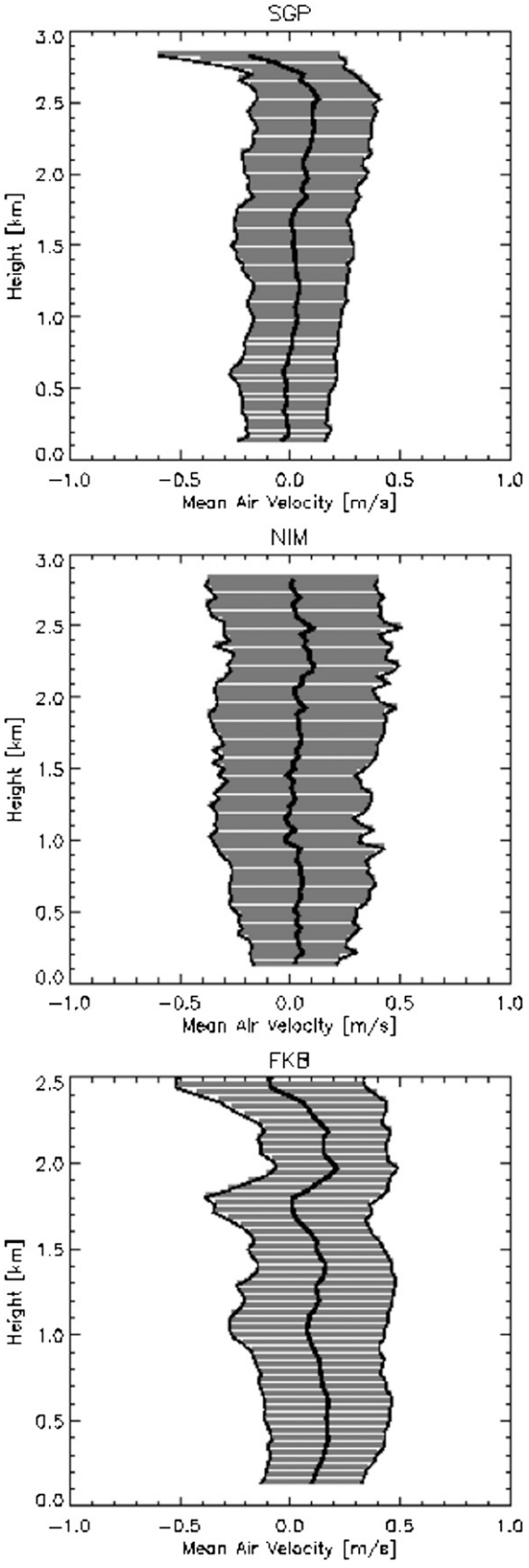

disdrometer record at SGP is less reliable for insight into M246 methods, matched dual-frequency 35- and 95-GHz Doppler velocity observations at SGP offer a reference for the desirability of gamma treatments and consistency of retrieval methods.

2) Additional challenges for automatic WACR methods

When attempting automatic retrievals for the Germany AMF deployment, one noteworthy development obstacle was an apparent regional pitfall toward using non-Rayleigh spectral signatures at light–moderate rainfall rates (Figs. 2 and 4). The automatic spectra retrievals as in Giangrande et al. (2010) are contingent on the availability of pronounced non-Rayleigh spectra signatures in rain to designate a ''minimum'' location between spectral peaks using wavelet techniques. For modest rainfall rates near 5–10 mm h^{-1}, expectations for the bi- or multimodality of the Doppler spectra (e.g., designating a non-Rayleigh minimum) were frequently challenged (as in Figs. 2 and 4 for the 8 August 2007 FKB event, a more pronounced single peak was observed). For a properly functioning radar system, changes in bulk drop size availability (e.g., higher concentrations of smaller drops) would explain an overall lack of prominent spectral bi- or multimodality at comparable rainfall rates. For example, in comparison with Fig. 1 for Niamey wherein multiple peak observations are commonplace, the spectral observations at FKB for surface rainfall rates at or exceeding 5 mm h^{-1} rarely demonstrate a pronounced second spectral peak. These examples were included to alleviate possible concerns that smaller median drop sizes at FKB were a consequence of retrieval error.

3. Results

Vertical air velocity mean and standard deviation calculations are presented in Fig. 5 for the SGP, NIM, and FKB deployments (top, middle, and bottom panels, respectively). A weak downward trend in air motion is recorded at all locations. Based on arguments from the previous section, a slight underestimation of downward air motions at altitude is possible if standard Foote and du Toit (1969) corrections hold. However, the observation is still to within the 10–20 cm^{-1} accuracy tolerance

←

FIG. 5. Profile of the mean and standard deviation of hourly averaged vertical air velocity retrievals for the (top) SGP, (middle) NIM, and (bottom) FKB ARM WACR cloud radar deployments. Positive values indicate downward air motion.

defined for instantaneous WACR retrievals (Giangrande et al. 2010). Standard deviations in Fig. 5 are those determined from the time series of the hourly mean velocity values for a particular height and typically to within 0.25 m s^{-1}. For instantaneous observations as following Giangrande et al. (2010), the mean profiles are unchanged and the standard deviation is to within 0.5 m s^{-1} (not shown). The percentages of instantaneous velocity observations in excess of 1 and 2 m s^{-1} are typically below 5% and 1%, respectively.

The near-surface (120 m) histograms of D0 for three different surface rainfall rate intervals—$1 < R < 3$ mm h^{-1}(thick line), $3 < R < 5$ mm h^{-1} (thin line), and $5 < R < 10$ mm h^{-1} (dashed line)—are shown in Figs. 6a–c (for SGP, NIM, and FKB, respectively). Mean D0 values increase with increasing rainfall rate at FKB and SGP (1.4, 1.45, and 1.49 mm at FKB; 1.43, 1.58, and 1.61 mm at SGP), as indicated in the plots. An exception to this behavior is at the tropical NIM site wherein the overall values are typically higher (1.65, 1.67, and 1.53 mm), but the histograms are less defined and the smallest D0 values are observed at the most intense of the rainfall rate intervals we examine.

The vertical structure of D0 profiles under the surface rainfall rate conditions described above is shown in Figs. 6d–f. These data are filtered using a 0.5 km × 1 min DSD aggregation–concatenation window. That is, rather than a simple averaging of instantaneous DSD retrieval values, the instantaneous DSD retrievals are power weighted according to relative drop number contributions by assuming the known surface rainfall rate is constant over this filtering window. Our averaging of DSDs serves two specific purposes. First, the degradation of WACR observations to larger sampling windows facilitates comparisons of the D0 profile variability for the volumes expected from platforms with large (~1 km^3) footprints (e.g., spaceborne and ground-based radars). Second, recent studies show the benefits of concatenating or nonsequential sampling DSDs as a function of similar rainfall rate and other DSD characteristics to help reduce random system (e.g., miscalibration) and some physical process noise (e.g., Lee and Zawadzki 2005; Cao and Zhang 2009). Single-parameter averaging over a long dataset (e.g., averaging solely based on a common rain-rate interval) might reduce the random system noise, but this does not mitigate the mixing of physical processes in time. For spaceborne retrievals, however, this sort of large-volume and multiprocess contamination is relevant and we calculate the standard deviations of the 1-min D0 profile values about the overall mean profile for an indication of this variability error.

Averaged D0 profiles in Fig. 6 indicate an increase in D0 from the base of the melting layer to the surface. The increase is to within 0.1 mm for all sites. Since the standard deviation was found to be a near constant with height–rainfall rate, this value is represented by a single error bar for each plot. From these plots, it is shown that the spread of 1-min profile D0 observations about these averaged conditions ranged from 0.3 mm (FKB, SGP) to 0.4 mm (NIM).

In addition to WACR spectra-based D0 retrieval efforts, collocated WACR-MMCR 35–95-GHz radar systems at SGP allow for additional insights into WACR retrieval consistency and the validity of Doppler velocity-based D0 retrievals in stratiform conditions [e.g., as in Tian et al. (2007) for 10–95 GHz and in Munchak and Tokay (2008) for 13–35 GHz], relevant for planned spaceborne dual-frequency radar platforms. Figure 7a plots MMCR and WACR mean Doppler velocity values at the lowest matched gate (120 m) as a histogram contoured according to observation pair counts. Selection of this gate was made to mitigate errors that might stem from air density corrections, attenuation in rain, and radar volume mismatch. As in Fig. 7a, Doppler velocity values are observed to be well matched (along a 45° line) to near 3.0 m s^{-1}. That is, these well-matched velocity values suggest a Rayleigh scattering regime situation at both wavelengths. Differences in velocity values linked to non-Rayleigh scattering at 35–95 GHz imply the presence of drops that are larger than 1 mm with known fall speeds >4 m s^{-1}. Better agreement is again found at higher velocities (>6.5 m s^{-1}) and reflects the case of non-Rayleigh resonance expectations for the backscatter cross section of now-present larger-sized drops at 35 GHz.

Several studies discuss the potential for dual-frequency radar observations for liquid water content retrievals [e.g., differential attenuation techniques, as in Hogan et al. (2005) and others] as well as D0 retrievals that operate by mapping mean Doppler velocity differences to particular DSD model patterns of behavior (e.g., Tian et al. 2007; Munchak and Tokay 2008). The latter dual-frequency methods are often considered as there is an expectation that bulk mean Doppler velocity moments are unaffected by partial attenuation in rain (as with non-Rayleigh spectral signatures). Figure 7b plots theoretical DSD expectations (exponential, dashed with $\mu = 0$; gamma, solid with $\mu = 6$) for the difference ($V_{35\text{-GHz}} - V_{95\text{-GHz}}$) of the mean Doppler velocity against an associated D0 as in (2). Here, we have ignored the implications of mean air motion (e.g., updrafts–downdrafts) and turbulence since it is assumed these measurements are well matched. The multiple curves represent cursory truncations for a maximum available drop diameter, Dmax (1.5, 2.00, and 3+ mm), wherein it is intuitive that prescribing smaller maximum drop diameters necessitates

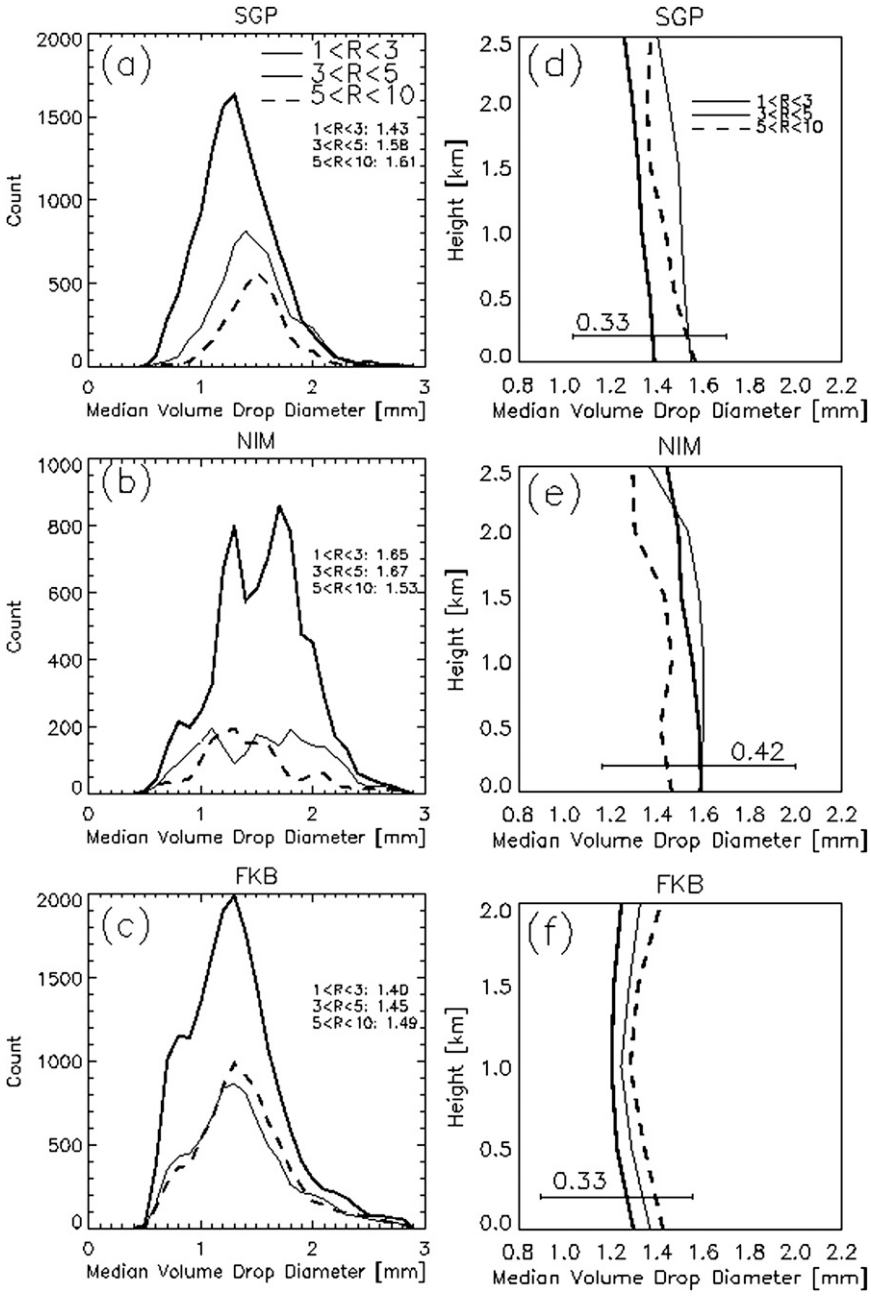

FIG. 6. WACR-based retrievals of the median volume drop diameter D0 at the lowest available range gate (120 m) for the (a) SGP, (b) NIM, and (c) FKB deployments, respectively. Rainfall rate segregation is performed for $1 < R < 3$ mm h^{-1} (thick solid), $3 < R < 5$ mm h^{-1} (thin solid) and $5 < R < 10$ mm h^{-1} (dashed) intervals, with associated mean values listed. (d)–(f) Profiles of D0 with associated standard deviation, segregated according to rainfall rates as in (a)–(c).

following along lower D0 curves for a predefined DSD model. Note, smaller Dmax truncation curves are intended only as a first-order reference to a potential sensitivity of mean Doppler velocity calculations at the 35–94-GHz pairing to the availability of certain drop sizes as a function of radar wavelength along a given DSD model.

Dual-frequency Doppler velocity observations at the SGP site offer reference for the consistency of spectral-based WACR D0 retrievals. Figure 7b also overlays the

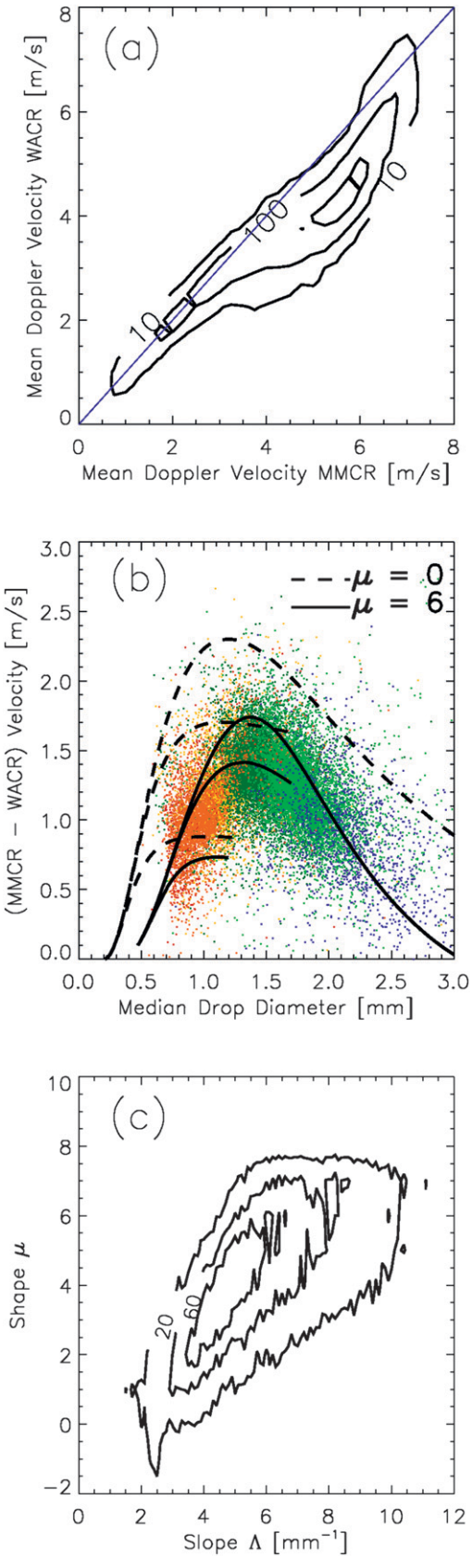

observed difference of mean Doppler velocity against WACR retrievals of D0. The observations have been color coded to identify slower (red and orange, 4–5 m s^{-1}) to faster (green and blue, 6–7 m s^{-1}) absolute magnitudes of the MMCR mean Doppler velocity (proxy for availability of larger drop sizes). As an additional reference, Fig. 7c plots the histogram of the corresponding slope-shape pairs for the associated retrievals.

4. Discussion and conclusions

Widespread light to moderate precipitation from three climatologically different regimes is investigated using an established retrieval technique based on resonance effects on 95-GHz radar Doppler spectra. Vertical air motion statistics are consistent across various climatic regions and generally indicate a preferential, weak downward motion beneath the melting layer. Standard deviations are to within 0.25 m s^{-1} for hourly averaged retrievals. Results are consistent with the velocity structures from other radar or wind profiler efforts, including Yuter and Houze (1995) and Cifelli et al. (2000) for stratiform events. However, since the behavior of the mean velocity is to within the known uncertainties of the retrievals, the conclusion is that mean air motions in widespread precipitation are near zero with infrequent excursions in excess of 0.25 m s^{-1} in magnitude. Here, the AMF retrieval dataset provides additional documentation of the vertical air motion field consistent with our current understanding of stratiform precipitation dynamics.

For the continental SGP and orographic FKB regions, increases in rainfall rate suggest slight increases in D0. In particular, FKB has the smallest relative D0 values for all conditions tested. This is consistent with the spectral observations in Figs. 1–4 and the observation of Doppler spectra with marginal non-Rayleigh signatures that indicates a relative lack of drops larger than 1–2 mm.

←

FIG. 7. (a) Mean Doppler velocity contours (2D histogram counts) for MMCR and WACR observations from the SGP deployment during May 2007. (b) Difference (MMCR − WACR) of cloud radar Doppler velocity vs WACR-retrieved median volume drop diameter (dots). Rainbow color shading indicates 0.5 m s^{-1} increases in the magnitude of the MMCR mean Doppler velocity from 4 (red) to greater than 7 m s^{-1} (dark blue). Overlain solid and dashed curves show theoretical expectations for gamma distributions of shape parameters $\mu = 6$ and $\mu = 0$ (exponential). Curve iterations reflect the impact on velocity difference with changes to the simulated maximum diameter: 1.5, 2, and 3.0 mm, respectively. (c) The 2D histogram counts of gamma shape and slope parameters for the associated velocity locations in (a) and (b).

Smaller relative D0 values and the absence of larger drops may be associated with orographic uplift at FKB, or may be favorable for the sort of shallow FKB events in our warm-season dataset of presumed limited coalescence, aggregation, and/or evaporation.

The tropical NIM dataset exhibited the largest relative D0 values at low rainfall rates <5 mm h^{-1}. As rainfall rate thresholds increased (still to within light–moderate intensity), NIM D0 values decreased to below those observed at the SGP site. Previous West African studies have suggested an absence of smaller drops during similar conditions (Sauvageot and Lacaux 1995; Nzeukou et al. 2004), although the use of impact disdrometers in those studies is also consistent with their results. Furthermore, interpretation for Niamey is challenging since preferential sampling (catching peripheries of convective cores) may also be the primary source of a smaller median drop size character at more intense ''stratiform'' rainfall rates. In the example of deep tropical convection provided in Figs. 1 and 3, it is shown that mature trailing stratiform regions with modest rainfall rates are associated with aggregation and well-defined multimodal spectra, suggesting increasingly larger drops sampled by the WACR. However, regions near the convective core at similar or higher rainfall rates by comparison demonstrate the relative absence of larger drops contributing, as illustrated by an absence of multiple spectral peaks at those times.

Characteristic D0 profiles for the selected light–moderate rainfall rate intervals are determined using an assumption that some physical process and random system noise can be minimized through rainfall-rate interval averaging. The standard deviation of the values about those averaged profiles (for a given rainfall-rate interval) indicates the variability such that a 1-km^3 volume may sample as a consequence of physical process (sorting) noise. The standard deviation of the 1-min values about these mean profiles was observed to be nearly constant with height–rainfall rate, ranging from 0.3 mm (FKB and SGP) to 0.4 mm (NIM). The observation that the largest 1-min measurement variability about our mean D0 profiles was observed at Niamey is reasonable considering previous discussions on the high diversity of spectral characteristics at light rainfall rates through typical tropical deep convective storms. The increase in D0 from the base of the melting layer to the surface is subtle and to within 0.1 mm at all locations. This type of behavior is not inconsistent with expectations for DSD evolution (e.g., coalescence) toward the surface, but the evidence for this gradual 0.1-mm change (even if averaged to reduce random noise) is limited provided standard non-Rayleigh slope retrieval accuracy to roughly 2–3 cm^{-1}, as reported by Giangrande et al. (2010) and others. Profile behavior is comparable to histograms for Darwin stratiform events found in Cifelli et al. (2000) with minor D0 shifts according to apparently regional changes in DSDs (e.g., smaller relative drop sizes at FKB).

Combined dual-frequency Doppler velocity observations and WACR spectral-based retrievals provide added insights into the use and internal consistency for use of gamma retrievals to explain observations at the SGP site. Mean Doppler velocity characteristics indicate an exponential DSD model is apparently insufficient to capture the bulk of this SGP velocity dataset in that magnitudes of the observed mean MMCR − WACR Doppler velocity difference question the validity of exponential models at these matched volumes and scales, especially nontruncated approaches. Treatment of small drop populations and Dmax appear to be critical at these wavelengths, especially when accounting for observed Doppler velocity pairings that specifically indicate offsetting resonance effects. For example, we find numerous SGP pairs that, according to Fig. 7, indicate relatively low differential velocity values $\sim$0.75 m s^{-1} and modest magnitudes of the MMCR (or WACR) mean Doppler velocities $>$6–7 m s^{-1}. These observations favor DSD modes having a positive shape factor 0f $\mu \sim 6$, or lower shape factors with more appropriate Dmax treatments. From the scatterplot in Fig. 7c, the corresponding WACR retrievals (truncated, M246) for the SGP indicate shape factors of $2 < \mu < 6$, where the retrievals reflect some truncation to WACR spectra limits as in Giangrande et al. (2010). This demonstrates solid internal consistency with what DSDs may be required to match differential velocity observations, but these efforts are limited as they are not a direct comparison with another instrument capable of small–large drop sampling. Additional study must also be performed to determine if some more-pronounced gamma pairings (relatively low slope values paired with higher shapes) are simply related to fitting patterns of DSD behavior at the short 2-s Doppler velocity-type intervals that are more apt to capture finer-scale sorting effects.

A practical target for future spaceborne dual-frequency radar systems is D0 retrievals that capitalize only on bulk velocity moments (requiring Doppler velocity pairings and a reference to D0 values from WACR or a disdrometer). Our observations at 35–95 GHz follow the efforts of others at different frequencies (e.g., Tian et al. 2007). We echo that there exists significant, but perhaps not sufficient, information for D0 retrievals at 35–95-GHz velocity pairings as compared with non-Rayleigh methods or other surface-based sensors. The magnitude of the MMCR velocity (Fig. 7b, colored points) is often sufficient to narrow the selection of a particular solution if a DSD model is prescribed. Again, one complication is a

potential sensitivity of the mean Doppler velocity to natural limitations including Dmax. Since the 35-GHz Ka-band mean Doppler velocity is more sensitive to the presence of larger drop sizes, poor DSD model behavior patterns at the larger size imply added variability in mean Doppler velocity than at W band for similar D0 conditions. Ambient air motions will also complicate these efforts, as updrafts or downdrafts can introduce variabilities of up to 0.25–0.5 m s^{-1}, which are sufficient to render individual Doppler velocity measurements of limited use.

Future efforts to improve velocity and DSD retrievals (using spectra and dual-frequency methods) must continue to address uncertainties in the presented methodology and the representativeness of 95-GHz radar observations as compared with known surface–profiling platforms. The 2009 American Recovery and Reinvestment Act (ARRA) U.S. Department of Energy (DOE) ARM and AMF site enhancements (as well as recent 2011 ARM DOE field campaign efforts with NASA GPM) included the purchase and placement of multiple video disdrometers with dual-frequency scanning cloud radars at the 95- and 35-GHz frequencies. Additional support was provided for collocation of a Doppler lidar and dual-frequency wind profilers at the SGP location. First, efforts are ongoing toward the use of Doppler lidar in precipitation studies as an additional reference for 95-GHz velocity retrievals for light to moderate rain conditions (e.g., Träumner et al. 2010). Since Doppler lidar may help to designate aerosol (passive tracer) air motions that are immune to terminal velocity air density corrections at altitude, longer-term analyses of joint Doppler lidar and 95-GHz spectral datasets in appropriate rain conditions provide one path for exploring W-band retrieval accuracy and better interpreting altitude corrections as in section 2. Similarly, collocation with video disdrometers may also provide a better surface anchor reference for the behavior of gamma versus exponential parameter retrieval methods and the range of drop sizes captured by the ARM WACR or comparable W-band systems.

Acknowledgments. This research was supported by the Office of Science (BER), U.S. Department of Energy. Data were obtained from the ARM archive. We thank our anonymous reviewers for helpful suggestions.

REFERENCES

Beard, K. V., 1985: Simple altitude adjustments to raindrop velocities for Doppler radar analysis. *J. Atmos. Oceanic Technol.,* **2,** 468–471.

Bringi, V. N., C. R. Williams, M. Thurai, and P. T. May, 2009: Using dual-polarized radar and dual-frequency profiler for DSD characterization: A case study from Darwin, Australia. *J. Atmos. Oceanic Technol.,* **26,** 2107–2122.

Campos, E., and I. Zawadzki, 2000: Instrumental uncertainties in *Z–R* relations. *J. Appl. Meteor.,* **39,** 1088–1102.

Cao, Q., and G. Zhang, 2009: Errors in estimating raindrop size distribution parameters employing disdrometer and simulated raindrop spectra. *J. Appl. Meteor. Climatol.,* **48,** 406–425.

Cifelli, R., C. R. Williams, D. K. Rajopadhyaya, S. K. Avery, K. S. Gage, and P. T. May, 2000: Drop-size distribution characteristics in tropical mesoscale convective systems. *J. Appl. Meteor.,* **39,** 760–777.

Foote, G. B., and P. S. du Toit, 1969: Terminal velocity of raindrops aloft. *J. Appl. Meteor.,* **8,** 249–253.

Giangrande, S. E., E. P. Luke and P. Kollias, 2010: Automated retrievals of precipitation parameters using non-Rayleigh scattering at 95 GHz. *J. Atmos. Oceanic Technol.,* **27,** 1490–1503.

Gunn, R., and G. D. Kinzer, 1949: The terminal velocity of fall for water droplets in stagnant air. *J. Meteor.,* **6,** 243–248.

Hogan, R. J., N. Gaussiat, and A. J. Illingworth, 2005: Stratocumulus liquid water content from dual-wavelength radar. *J. Atmos. Oceanic Technol.,* **22,** 1207–1218.

Houze, R. A., Jr., 1997: Stratiform precipitation in regions of convection: A meteorological paradox? *Bull. Amer. Meteor. Soc.,* **78,** 2179–2196.

Joss, J., and A. Waldvogel, 1967: Ein Spektrograph fur Niederschlagstrophen mit automatischer Auswertung (A spectrograph for the automatic analysis of raindrops). *Pure Appl. Geophys.,* **68,** 240–246.

Kollias, P., E. E. Clothiaux, M. A. Miller, E. P. Luke, K. L. Johnson, K. P. Moran, K. B. Widener, and B. A. Albrecht, 2007a: The Atmospheric Radiation Measurement Program cloud profiling radars: Second-generation sampling strategies, processing, and cloud data products. *J. Atmos. Oceanic Technol.,* **24,** 1199–1214.

——, W. Szyrmer, I. Zawadzki, and P. Joe, 2007b: Considerations for spaceborne 94 GHz radar observations of precipitation. *Geophys. Res. Lett.,* **34,** L21803, doi:10.1029/2007GL031536.

Kummerow, C., and Coauthors, 2000: The status of the Tropical Rainfall Measuring Mission (TRMM) after two years in orbit. *J. Appl. Meteor.,* **39,** 1965–1982.

L'Ecuyer, T. S., and G. L. Stephens, 2002: An estimation-based precipitation retrieval algorithm for attenuating radars. *J. Appl. Meteor.,* **41,** 272–285.

Lee, G. W., and I. Zawadzki, 2005: Variability of drop size distributions: Noise and noise filtering in disdrometric data. *J. Appl. Meteor.,* **44,** 634–652.

Lhermitte, R., 1987: A 94-GHz Doppler radar for cloud observations. *J. Atmos. Oceanic Technol.,* **4,** 36–48.

——, 2002: *Centimeter and Millimeter Wavelength Radars in Meteorology*. Lhermitte Publications, 550 pp.

Masunaga, H., and C. D. Kummerow, 2005: Combined radar and radiometer analysis of precipitation profiles for a parametric retrieval algorithm. *J. Atmos. Oceanic Technol.,* **22,** 909–929.

Miriovsky, B. J., and Coauthors, 2004: An experimental study of small-scale variability of radar reflectivity using disdrometer observations. *J. Appl. Meteor.,* **43,** 106–118.

Munchak, S. J., and A. Tokay, 2008: Retrieval of raindrop size distribution from simulated dual-frequency radar measurements. *J. Appl. Meteor. Climatol.,* **47,** 223–239.

Nzeukou, A., and Coauthors, 2004: Raindrop size distribution and radar parameters at Cape Verde. *J. Appl. Meteor.,* **43,** 90–105.

Sauvageot, H., and J.-P. Lacaux, 1995: The shape of averaged drop size distributions. *J. Atmos. Sci.,* **52,** 1070–1083.

Steiner, M., R. A. Houze, and S. E. Yuter, 1995: Climatological characterization of three-dimensional storm structure from operational radar and rain gauge data. *J. Appl. Meteor.,* **34,** 1978–2007.

Tian, L., G. M. Heymsfield, L. Li, and R. C. Srivastava, 2007: Properties of light stratiform rain derived from 10- and 94-GHz airborne Doppler radars measurements. *J. Geophys. Res.,* **112,** D11211, doi:10.1029/2006JD008144.

Tokay, A., and D. A. Short, 1996: Evidence from tropical raindrop spectra of the origin of rain from stratiform versus convective clouds. *J. Appl. Meteor.,* **35,** 355–371.

——, and P. G. Bashor, 2010: An experimental study of small-scale variability of raindrop size distribution. *J. Appl. Meteor. Climatol.,* **49,** 2348–2365.

Träumner, K., J. Handwerker, A. Wieser, and J. Grenzhäuser, 2010: A synergy approach to estimate properties of raindrop size distributions using a Doppler lidar and cloud radar. *J. Atmos. Oceanic Technol.,* **27,** 1095–1100.

Vivekanandan, J., G. Zhang, and E. Brandes, 2004: Polarimetric radar rain estimators based on constrained gamma drop size distribution model. *J. Appl. Meteor.,* **43,** 217–230.

Williams, C. R., W. L. Ecklund, P. E. Johnston, and K. S. Gage, 2000: Cluster analysis techniques to separate air motion and hydrometeors in vertical incident profiler observations. *J. Atmos. Oceanic Technol.,* **17,** 949–962.

Wulfmeyer, V., and Coauthors, 2008: The Convective and Orographically Induced Precipitation Study: A research and development project of the World Weather Research Program for improving quantitative precipitation forecasting in low-mountain regions. *Bull. Amer. Meteor. Soc.,* **89,** 1477–1486.

Yuter, S. E., and R. A. Houze Jr., 1995: Three-dimensional kinematic and microphysical evolution of Florida cumulonimbus. Part II: Frequency distributions of vertical velocity, reflectivity, and differential reflectivity. *Mon. Wea. Rev.,* **123,** 1941–1963.

Zrnić, D. S., 1975: Simulations of weather like Doppler spectrum and signals. *J. Appl. Meteor.,* **14,** 619–620.